# Cofactor assisted gating mechanism in the active site of NADH oxidase from Thermus thermophilus

**ARTICLE** *in* PROTEINS STRUCTURE FUNCTION AND BIOINFORMATICS · AUGUST 2006

Impact Factor: 2.63 · DOI: 10.1002/prot.20990 · Source: PubMed



**3 AUTHORS**, INCLUDING:

Jozef Hritz
CEITEC MU
**25** PUBLICATIONS **596** CITATIONS
SEE PROFILE

Erik Sedlák
Pavol Jozef Šafárik University in Košice
**53** PUBLICATIONS **886** CITATIONS
SEE PROFILE

PROTEINS: Structure, Function, and Bioinformatics 64:465–476 (2006)

# Cofactor Assisted Gating Mechanism in the Active Site of NADH Oxidase from *Thermus thermophilus*

**Jozef Hritz,[1,2] Gabriel Žoldák,[1] and Erik Sedlák[1]***

[1]*Department of Biochemistry, Faculty of Science P. J. Šafárik University, Košice, Slovakia*
[2]*Leiden/Amsterdam Center for Drug Research, Division of Molecular Toxicology, Vrije Universiteit Amsterdam, The Netherlands*

***ABSTRACT:*** **NADH oxidase (NOX) from *Thermus thermophilus* is a member of a structurally homologous flavoprotein family of nitroreductases and flavin reductases. The importance of local conformational dynamics in the active site of NOX has been recently demonstrated. The enzyme activity was increased by 250% in the presence of 1 M urea with no apparent perturbation of the native structure of the protein. The present *in silico* results correlate with the *in vitro* data and suggest the possible explanation about the effect of urea on NOX activity at the molecular level. Both, X-ray structure and molecular dynamics (MD) simulations, show open conformation of the active site represented by ~0.9 nm distance between the indole ring of Trp47 and the isoalloxazine ring of FMN412. In this conformation, the substrate molecule can bind in the active site without sterical restraints. MD simulations also indicate more stable conformation of the active site called "closed" conformation. In this conformation, Trp47 and the isoalloxazine ring of FMN412 are so close to each other (~0.5 nm) that the substrate molecule is unable to bind between them without perturbing this conformation. The open/close transition of the active site between Trp47 and the flavin ring is accompanied by release of the "tightly" bound water molecule from the active site—cofactor assisted gating mechanism. The presence of urea in aqueous solutions of NOX prohibits closing of the active site and even unlocks the closed active site because of the concomitant binding of a urea molecule in the active site cavity. The binding of urea in the active site is stabilized by formation of one/two persistent hydrogen bonds involving the carbonyl group of the urea molecule. Our report represents the first MD study of an enzyme from the novel flavoprotein family of nitroreductases and flavin reductases. The common occurrence of aromatic residues covering the active sites in homologous enzymes suggests the possibility of a general gating mechanism and the importance of local dynamics within this flavoprotein family. Proteins 2006;64:465–476.** © 2006 Wiley-Liss, Inc.

**Key words: molecular dynamics; flavoenzymes; thermophiles; activity; urea binding**



## INTRODUCTION

NADH oxidase (EC 1.6.99.3) (NOX) from *Thermus thermophilus* is a member of the novel structurally homologous flavoprotein family of flavin reductases and nitroreductases.[1–6] This family of nitroreductases attracts intense attention in medicine, industry, and environmental chemistry. Nitroreductases and homologous enzymes reduce substrates through a bi-bi ping-pong kinetic mechanism as observed in nitroreductases that reduced nitroaromatic to nitrosoaromatic compounds.[5–7] Nitrosoaromatic compounds in vivo undergo a subsequent nonenzymatic reaction cascade that results in production of highly cytotoxic agents capable of directly alkylating DNA.[8] The nitroreductases are suitable tools for gene therapy, for the tumor selective activation of alkylating drugs in gene-directed enzyme-prodrug therapy.[9] The FMN-dependent nitroreductase from *Escherichia coli* has been used in clinical trials for virus-directed therapy with various prodrugs such as CB1954 [5-(aziridin-1-yl-)-2,4 dinitrobenzamide].[10] Furthermore, nitroreductases participate in the detoxification of explosive contaminants such as 2,4,6-trinitrotoluene and 4,6-dinitrobenzofuroxan[11,12] and thus decrease environmental contamination from explosives. The ability to modulate (inhibit or activate) the activity of the flavin reductases and nitroreductase is of interest to medicinal and biotechnological researchers.

How similar are the flavoenzymes from this family? The sequence alignment shows that the pair-wise sequence identity is not very high even between homologous flavoproteins.[3,4] However, the crystal structures of the homologous

*Abbreviations:* NOX, NADH oxidase; *T. thermophilus*, *Thermus thermophilus*; MD, molecular dynamics; PME, Particle Mesh Ewald; RMSD, root-mean-square deviation; Rg, radius of gyration; SAS, solvent accessible surface; CD, circular dichroism; FMN, flavin mononucleotide; FAD, flavin adenine dinucleotide; NADH, nicotinamide adenine dinucleotide; SPC, Simple Point Charge model.

The Supplementary Material referred to in this article can be found at http://www.interscience.wiley.com/jpages/0887-3585/suppmat/

Grant sponsor: Slovak Grant Agency; Grant number: 1/0432/03; Grant sponsor: HPC-Europe; Grant number: RII3-CT-2003-506079.

*Correspondence to: Erik Sedlák, Department of Biochemistry, Faculty of Science P.J. Šafárik University, Moyzesova 11, 040 01 Košice, Slovakia. E-mail: sedlak_er@saske.sk

Received 10 September 2005; Revised 30 December 2005; Accepted 13 February 2006

Published online 26 April 2006 in Wiley InterScience (www.interscience.wiley.com). DOI: 10.1002/prot.20990

enzymes show the common occurrence of aromatic residues (Phe, Trp, Tyr) covering the *re*-side of the flavin ring, partly burying the flavin ring, and decreasing the solvent/substrate accessibility. Moreover, the crystal structures of some nitro/oxidoreductases reveal that nicotinamide access to the isoalloxazine ring is blocked by an aromatic residue that needs to be displaced by the incoming substrate or inhibitor.[3,13–16] This indicates the active role of these aromatic residues as a gate serving to increase enzyme specificity or helping to push the product out of the active site.

NOX from *T. thermophilus* is stable in extremes of heat, pH, and chaotropic agent concentration.[17–21] The enzyme catalysis includes hydride transfer from NADH to the intrinsic flavin cofactor. The protein preferentially binds the FMN cofactor with an apparent $K_d \approx 10^{-7}$ M.[4] The intrinsic flavin cofactor is recycled by extrinsic cosubstrates such as FMN and FAD. Recent investigations demonstrated that the presence of a chaotropic reagent such as urea, anions of the Hofmeister series, and pH changes produce an enhancement of the activity of NOX at room temperature.[17–19] Based on the experimental data and the structure analysis, we suggested that the local movement of the indole ring of Trp47, located in the active site of the enzyme, can be the reason for the increase in enzyme activity in the presence of urea.[17]

In an effort to elucidate the detailed molecular mechanism of the modulation of NOX activity by urea molecules, an MD simulation was performed in two different solvent conditions, water solution and 1 M urea. The molecular modeling results indicate how binding of the urea molecule in the enzyme active site can lead to increase in the activity of NOX from *T. thermophilus* at room temperature.

## MATERIALS AND METHODS

### Structure of NOX From *T. thermophilus*

The crystal coordinates for the dimer of NOX from *T. thermophilus*[4] is from the Brookhaven Protein Data Bank[22] (filename: 1NOX.pdb). This file also contains a list of B-factors for each atom. The homodimeric structure contains the protein moiety and two molecules of the flavin cofactor FMN. The initial N-terminal sequence, Met-Glu-Ala-Thr-Leu, is missing in the published crystal structure. We have added it for stability reasons during the MD runs. For the protein with bound molecules of FMN, the extended-atom GROMOS-96 force field[23] was used, as implemented in the GROMACS MD simulation package.[24,25] GROMOS-96 force field set contains standard building blocks for amino acids and for other related molecules (cofactors). In our simulations, we have used a standard GROMOS-96 building block "[FMNO]" for the flavin mononucleotide in the oxidized state.

The water was modeled as standard SPC.[26] The counterions $Na^+$ and $Cl^-$ were added to electroneutralize the whole system. We have used a solution composed of 9,900 water molecules, 181 urea molecules, 50 counterions of $Na^+$ and 54 counterions of $Cl^-$ for the simulation of NOX in 1 M urea. Positions of 181 added urea molecules were randomly generated over a simulation box except the volume occupied by NOX.

### Molecular Modeling

We run three different sets of MD simulations: 1. NOX in water solution starting from the crystallographic conformation, 2. NOX in 1 M urea solution starting from the crystallographic conformation, 3. NOX in 1 M urea solution starting from the state in which the catalytic site is in the closed conformation. Each of these MD simulation sets contains 10 independent MD runs (different initial atom velocities) of the length of 12 ns. In eight of them, electrostatic interactions were treated by the reaction-field method, three were prolonged up to 18 ns time length, and in two extra runs electrostatic interactions were treated by PME.

All MD simulations were conducted using the GROMACS MD simulation package (Version 3.2.1) running on a linux cluster. The Verlet integration scheme (leap-frog) was used with a time step of 2 fs.[27] Periodic boundary conditions, with a rectangular box, were applied to avoid edge effects. The LINCS algorithm was used to constrain all covalent bonds in nonwater molecules.[28] The SETTLE algorithm was used to constrain the bond lengths and angles in the water molecules.[29] After a steepest descent minimization to remove bad contacts between molecules, the initial velocities were randomly assigned from the Maxwell-Boltzmann distribution at 298 K, according to the atomic masses. The temperature was controlled using a weak coupling to a bath of 298 K with a time constant of 0.1 ps.[30] The protein with bound FMN molecules and solvent (i.e., water, counterions, and urea) were independently coupled to the heat bath. The pressure was controlled using isotropic weak coupling to atmospheric pressure with a time constant = 1.0 ps.[30] The van der Waals interactions were modeled using a 6–12 Lennard-Jones potential. As default, the van der Waals and electrostatic interactions were calculated using a triple range scheme. Interactions within a short-range cutoff of 0.9 nm were calculated every time step from a pairlist that was generated every five steps. At these time points, interactions between 0.9 and 1.4 nm were also calculated and kept constant between updates. A reaction-field contribution was added to the electrostatic interactions and forces to account for homogeneous medium outside the long-range cutoff, using the experimental value for the relative permitivity of water.[31] One of the principal reasons for the treatment of long-range electrostatic interactions by the reaction-field method is that all used GROMOS-96 force field parameters were derived by using this approach. To test that the observed phenomena are not biased by applying of the reaction-field method, we have run two extra simulations runs in which electrostatics was treated by PME algorithm,[32] with a 0.9 nm cut-off for the direct space calculation. The reciprocal space calculation was performed using a fast Fourier transformation algorithm.

Rg was calculated using the program g_gyrate implemented in the GROMACS MD simulation package as follows:

$$R_g = \sqrt{\left(\frac{\sum_i m_i \|\vec{r}_i\|^2}{\sum_i m_i}\right)} \quad (1)$$

where $\vec{r}_i$ is the position vector of an atom $i$ and $m_i$ is mass of atom $i$.

The RMSD of backbone atoms ($N_i$—$CA_i$—$C_i$—) in NOX with respect to the reference structure was calculated using the program g_rms (from GROMACS package) by least-square fitting the structure to the initial reference structure and subsequently calculating the RMSD by equation:

$$\mathrm{RMSD}(t) = \sqrt{\frac{\sum_i (m_i \|\vec{r}_i(t) - \vec{r}_i(0)\|^2)}{\sum_i m_i}} \quad (2)$$

where $\vec{r}_i(t)$ is position vector of backbone atom $i$ at time $t$.

For the RMSD analysis of the secondary structure elements we have chosen (i) 9 α-helices: helix A (10–16), helix B (30–40), helix C (60–69), helix D (74–78), helix E (89–94), helix F (107–121), helix G (125–149), helix H (162–169), helix I (198–201); (ii) 4 β-sheets: sheet 1 (52–57), sheet 2 (81–87), sheet 3 (153–157), sheet 4 (179–184); and (iii) four loops (of size >9 residues): loop 1 (41–51), loop 2 (95–106), loop 3 (170–178), loop 4 (185–197).

B-factor for the $i$-th atom was calculated from MD trajectories by the program g_rmsf implemented in GROMACS MD simulation package according the following equation:

$$B_i = \left(\frac{8\pi^2}{3}\right)(\vec{r}_i - \langle\vec{r}_i\rangle^2) \quad (3)$$

where $\langle\vec{r}_i\rangle$ is mean value of the position vector of an atom $i$.

We have used only backbone atoms ($N_i$—$CA_i$—$C_i$—) for B-factors analysis to compare global conformational flexibility. The initial flexible region (residue numbers 1–5) was excluded from our B-factors analysis because it is not presented in crystallographic structure. Before comparison, B-factors from crystal structures and MD were normalized according Carugo and Argos[33]:

$$B_{normalized} = \frac{(B - \langle B\rangle)}{\sigma}, \quad (4)$$

where $\langle B\rangle$ is mean value B-factor and σ is standard deviation of the B-factors. Pearson's correlation coefficient was calculated between B-factors as follows:

$$r = \frac{\sum B_i B_j - \frac{\sum B_i \sum B_j}{N}}{\sqrt{\left(\sum B_i^2 - \frac{(\sum B_i)^2}{N}\right)\left(\sum B_j^2 - \frac{(\sum B_j)^2}{N}\right)}} \quad (5)$$

where $B_i$, $B_j$ are B-factors from X-ray structure and MD in water; and MD in water and 1 M urea, respectively.

Calculation of the SAS was performed using the program g_sas implemented in the GROMACS MD simulation package. According to the original definition, SAS is the surface that is traced by the center of the sphere of radius 0.14 nm as it rolls on the van der Waals surface of the molecule.[34] Secondary structure analysis of protein was done using the DSSP program.[35]

The MD trajectories as well as the static structures were visualized using VMD molecular visualizer and POV-Ray renderer (http://www.povray.org).[36]

### Multiple Sequence Alignment

Sequence of NOX from *T. thermophilus* was submitted to BLASTp to find sequences producing significant alignments in the nonredundant databases. Scoring functions and similarities between amino acids were calculated using the Blosum62 matrix with the following gap penalties: for existence of the gap, 11 points and for extension of the gap, 1 point. Only sequences with the E-value of <1 were used. Only single sequence from multiple bacterial strains was taken into account. Sequences larger than 300 amino acids were excluded. Finally, we have obtained 67 sequences as follows: (1) NADH oxidase from *T. thermophilus*, (2) NADH oxidase *Thermus aquaticus*, (3) nitroreductase from *Deinococcus radiodurans* R1, (4) NADH dehydrogenase from *Deinococcus geothermalis* DSM 11300, (5) nitroreductase from *Desulfitobacterium hafniense* DCB-2, (6) nitroreductase from *Thermoanaerobacter ethanolicus* ATCC 33223, (7) probable NAD(P)H nitroreductase *Natronomonas pharaonis* DSM 2160, (8) nitroreductase from *Thermoanaerobacter tengcongensis* MB4, (9) nitroreductase from *Anabaena variabilis* ATCC 29413, (10) all1864 from *Nostoc* sp. PCC 7120, (11) NAD(P)H nitroreductase from *Symbiobacterium thermophilum* IAM 14863, (12) NAD(P)H nitroreductase from *Bacillus cereus* ATCC 14579, (13) nitroreductase from *Nostoc punctiforme* PCC 73102, (14) nitroreductase from *Desulfuromonas acetoxidans* DSM 684, (15) NAD(P)H nitroreductase from *Bacillus thuringiensis serovar konkukian* str. 97-27, (16) hypothetical protein BSU05660 from *Bacillus subtilis* str. 168, (17) related to nitroreductase from *Desulfotalea psychrophila* LSv54, (18) nitroreductase *Microbulbifer degradans* 2-40, (19) putative dehydrogenase from *Corynebacterium diphtheriae* NCTC 13129, (20) nitroreductase from *Magnetococcus* sp. MC-1, (21) NAD(P)H nitroreductase from *Bacillus clausii* KSM-K16, (22) nitroreductase-like from *Desulfovibrio desulfuricans* G20, (23) NADH dehydrogenase from *Bacillus halodurans* C-125, (24) NADH oxidase from *Archaeoglobus fulgidus* DSM 4304, (25) NAD(P)H-flavin oxidoreductase from *Paenibacillus polymyxa*, (26) nitroreductase family protein from *Bradyrhizobium* sp. BTAi1, (27) AGR_L_768p from *Agrobacterium tumefaciens* str.

C58, (28) nitroreductase from *Exiguobacterium* sp. 255-15, (29) NAD(P)H-dependent quinone reductase from *Streptococcus pyogenes* MGAS10394, (30) NAD(P)H-flavin oxidoreductase from *Thiobacillus denitrificans* ATCC 25259, (31) nitroreductase family protein from *Bdellovibrio bacteriovorus* HD100, (32) nitroreductase from *Streptococcus pneumoniae* R6, (33) putative oxidoreductase from *Gluconobacter oxydans* 621H, (34) nitroreductase from *Methanospirillum hungatei* JF-1, (35) nitroreductase from *Trichodesmium erythraeum* IMS101, (36) nitroreductase family protein from *Pelodictyon luteolum* DSM 273, (37) putative nitroreductase from *Nocardia farcinica* IFM 10152, (38) nitroreductase from *Pseudomonas aeruginosa* UCBPP-PA14, (39) nitroreductase from *Corynebacterium glutamicum* ATCC 13032, (40) nitroreductase from *Clostridium acetobutylicum* ATCC 824, (41) NAD(P)H-flavin oxidoreductase from *Staphylococcus epidermidis* ATCC 12228, (42) nitroreductase from *Bacillus anthracis* str. A2012, (43) nitroreductase from *Streptococcus mutans* UA159, (44) putative nitroreductase from *Campylobacter upsaliensis* RM3195, (45) nitroreductase from *Methylobacillus flagellatus* KT, (46) nitroreductase from *Azotobacter vinelandii*, (47) putative NADH oxidoreductase from *Thermotoga maritima* MSB8, (48) NAD(P)H-flavin oxidoreductase from *Wolinella succinogenes*, (49) putative nitroreductase from *Bordetella bronchiseptica* RB50, (50) nitroreductase from *Marinobacter aquaeolei* VT8, (51) nitroreductase from *Alkaliphilus metalliredigenes*, (52) nitroreductase from *Chloroflexus aurantiacus* J-10-fl, (53) nitroreductase from *Frankia* sp. EAN1pec, (54) DrgA gene product from *Synechocystis* sp. PCC 6803, (55) nitroreductase family protein from *Campylobacter jejuni* RM1221, (56) nitroreductase from *Moorella thermoacetica* ATCC 39073, (57) nitroreductase Cj1066 from *Campylobacter coli* RM2228, (58) nitroreductase from *Pseudomonas syringae* pv. syringae B728a, (59) nitroreductase family protein from *Methanosarcina mazei* Go1, (60) nitroreductase from *Enterococcus faeciumi*, (61) NADH oxidase from *Halobacterium* sp. NRC-1, (62) nitroreductase family protein from *Methylococcus capsulatus* str. Bath, (63) putative nitroreductase from *Bordetella parapertussis* 12822, (64) NADH dehydrogenase from *Aeropyrum pernix* K1, (65) nitroreductase family protein from *Geobacter sulfurreducens* PCA, (66) nitroreductase family from *Methanococcus maripaludis* S2, and (67) nitroreductase from *Actinobacillus pleuropneumoniae serovar* 1 str. 4074. ClustalW was used to perform global multiple sequence alignment using the progressive method [Fig. 2(A–D); see Supplementary Material (http://www.interscience.wiley.com/jpages/0887-3585/suppmat)].[37] Sequences with the highest sequence identity are aligned first and then additional sequences are added reflecting the initial alignments to produce a multiple sequence alignment. Sequence identity matrix is located in Figure 3 in Supplementary Material. We have calculated the following score from the obtained multiple sequence alignment:

$$\text{score} = \sum_{67} \omega_i X_i \tag{6}$$

where $\omega_i$ is weighting factor for the given amino acid equal to 1.0 or proportional to the number of codons, i.e., $\approx$ (number of codons)$^{-1}$ for the given aromatic amino acid and $X_i$ is equal to:

$$X_i = \begin{cases} 1 \text{ for } W,Y,F \\ 0 \text{ otherwise.} \end{cases} \tag{7}$$

The calculated score simply counts the number of aromatic residues at the alignment position for the multiple sequences. Weighting factor takes into account the different number of codons for phenylalanines, tyrosines, and tryptophans. Sequence of NOX was taken as a template for the position of the aromatic amino acids.

### Structural Alignment

Three-dimensional structure of the enzymes from the superfamily of nitroreductase, flavin reductase, and NOX was obtained from the Protein Data Bank.[38] We have obtained six published structures: (1) NOX from *T. thermophilus*—1nox.pdb, (2) NADPH:FMN oxidoreductase from *Vibrio harveyi*—1bkj.pdb, (3) NAD(P)H:FMN oxidoreductase from *Vibrio fisheri*—1vfr.pdb, (4) nitroreductase from *Enterobacter cloacae*—1nec.pdb, (5) FMN-dependent nitroreductase from *Escherichia coli* B—1ds7.pdb, and (6) oxygen-insensitive NADPH nitroreductase from *Escherichia coli*—1f5v.pdb. Structure based sequence alignments were performed by using Swiss-Pdb Viewer 3.7.

## RESULTS

### MD Simulations of NOX in Water

MD simulations were performed to investigate the behavior of NOX from *T. thermophilus* in water and in 1 M urea, i.e., conditions at which the maximal, 250%, enhancement of enzyme activity was observed.[17] Time evolutions of global structural parameters Rg and RMSD of the protein backbone indicate stability of NOX in water and 1 M urea solution during the whole time of MD simulations (Fig. 1). In both simulations, Rg of NOX was nearly constant over the time, $\langle Rg \rangle = 1.99$ nm. In addition, secondary structure of each residue over the time of simulations was calculated (Fig. 1 in Supplementary Material), which shows that their secondary structure remained stable during the whole time of MD simulations.

In an effort to analyze validity of MD simulations, they were compared with some independent experimental results. The suitable parameter is atomic displacement parameter termed thermal (Debye-Waller) B-factors.[39] Atomic displacement parameter describes amplitude of the atomic motion around equilibrium position or multiple positions.[39,40] This parameter was obtained from the trajectory of MD simulation and compared with the "experimental" B-factors from crystal structures. Similar patterns of the B-factors of backbone atoms are observed in water and also in the presence of 1 M urea. Pearson's correlation coefficient was calculated to compare normalized B-factors between data obtained from MD in water and X-ray structure (Fig. 2). The value of the coefficient, $r = 0.8491$, indicated a resemblance of the dynamics of

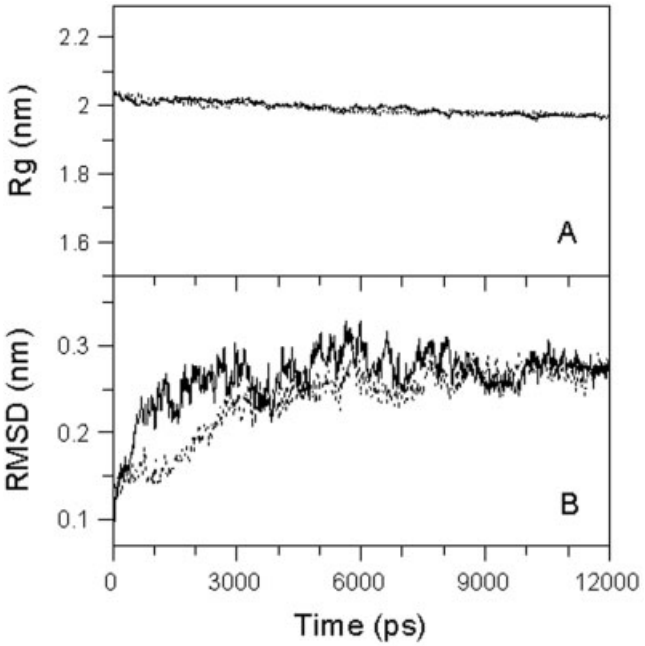


Fig. 1. Time dependences of (**A**) Rg of NOX and of (**B**) RMSD for backbone atoms and in water (solid line) and in 1 M urea solution (dotted line).

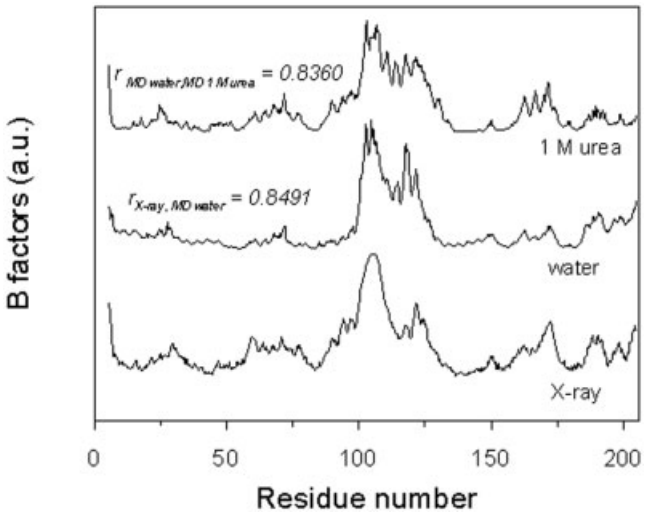


Fig. 2. Normalized B factors for backbone atoms (—$N_i$—$CA_i$—$C_i$—) from X-ray structure of NOX and MD simulation in water and 1 M urea solutions. Pearson's correlation coefficients ($r$) express the correlations between corresponding B factor profiles. Residues 1–5 were not included because of their absence in the crystal structure of NOX. For clarity, B factors from MD (water solution and 1 M urea) are shifted upward.

both structures. Similarity of B-factor profiles calculated from MD of NOX in water and 1 M urea solution ($r$ = 0.8360) showed that addition of urea into water solution of NOX did not significantly affect global flexibility during the time of simulation.

In the effort to analyze the influence of 1 M urea on the NOX structure in more detail, we have calculated time evolution of RMSDs of the 17 selected secondary structure elements. The majority of the RMSDs of secondary structure

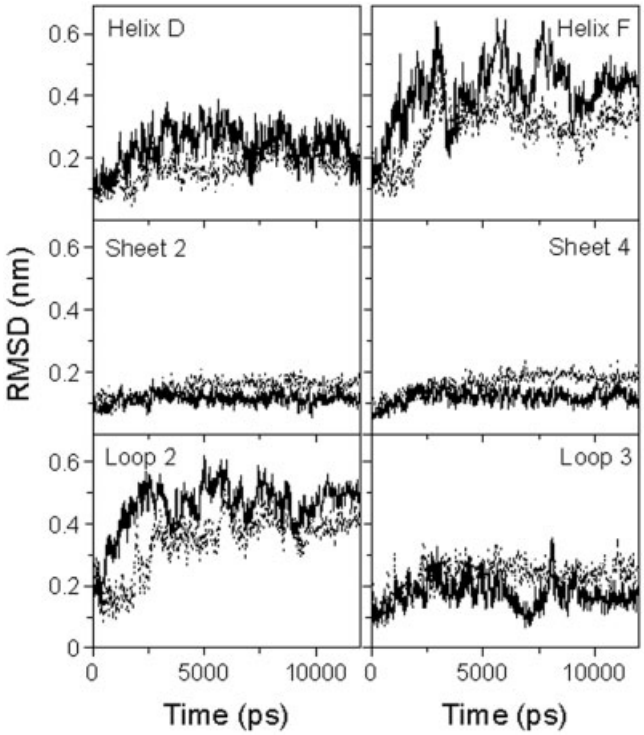


Fig. 3. Time dependences of RMSD of the selected secondary structure elements (helix D, helix F, sheet 2, sheet 4, loop 2, and loop 3) of NOX in water (solid line) and in 1 M urea solution (dotted line). RMSD of shown secondary structure elements are the most influenced in the presence of 1 M urea. The total number of analyzed secondary structure elements was 17 (nine α-helices, four β-sheets, and four loops; see Materials and Methods).

elements was not significantly affected in the presence of 1 M urea. The most affected time evolutions of RMSDs (for α-helix D, α-helix F, β-sheet 2, β-sheet 4, loop 2, and loop 3) are plotted in Figure 3. The protein core consists of the four antiparallel β-sheets. These β-sheets have the lowest value of RMSD indicating high rigidity of the protein core (Fig. 3). The presence of urea slightly increases RMSD values for all of β-sheets. α-Helices are more mobile than β-sheets. On average, RMSD of the helices is two times higher than that of β-sheets, ⟨RMSD⟩ ~0.2 nm for α-helices. ⟨RMSD⟩ of the most flexible helix F decreases from 0.41 to 0.30 nm after addition of 1 M urea. We have selected only four loops that have a size >9 and have approximately similar length. In the middle of the loop L2 is located Trp47. This loop is the most mobile secondary structure element, ⟨RMSD⟩ is 0.45 nm. The presence of urea decreases of the ⟨RMSD⟩ for loop L2 to the value 0.34 nm.

### Cofactor Assisted Gating Mechanism

In the crystal structure of NOX, both of the catalytic sites Trp47-FMN412 and Trp253-FMN206 are in the open conformation with the bound water molecule between the backbone NH group of the tryptophan residue and the hydroxyl group of the ribityl chain of flavin cofactor. This conformation was also observed in our MD simulations [Fig. 4(A)]. (Note: NOX is homodimer, therefore catalytic

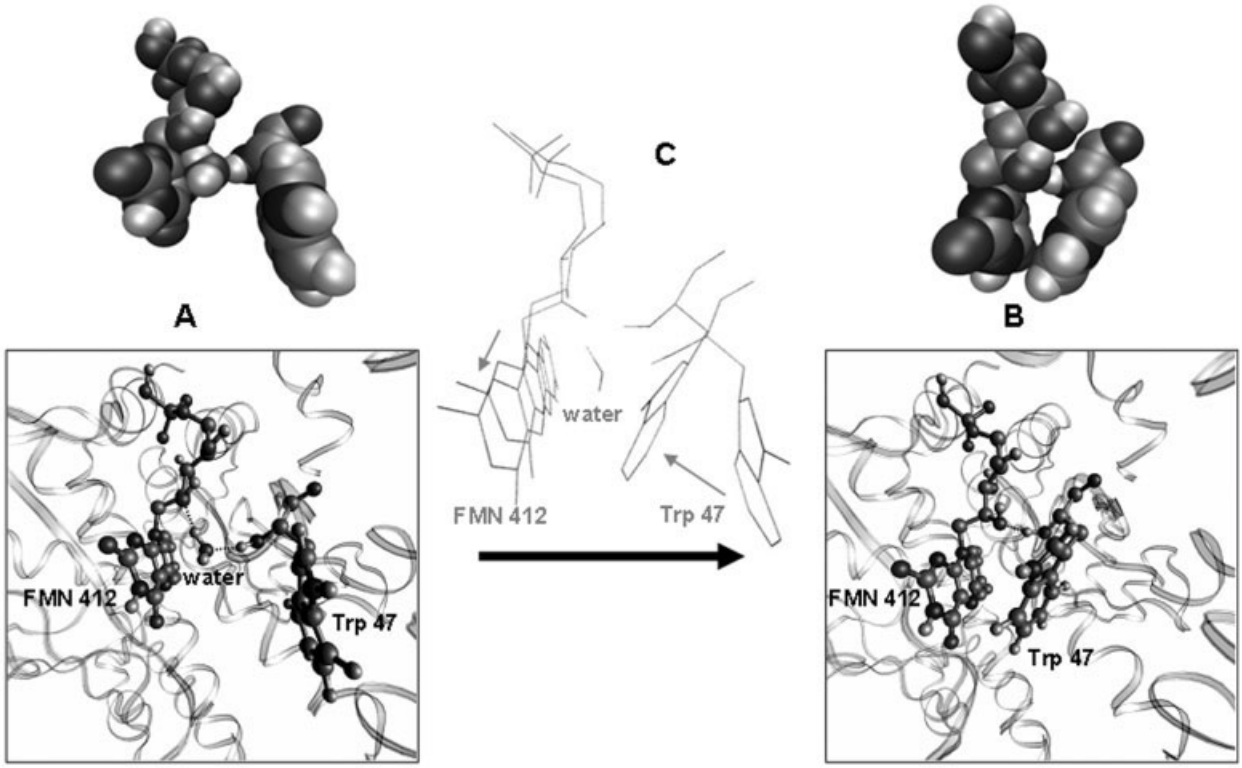


Fig. 4. Molecular model of the catalytic site of NOX in water. (**A**) Open and (**B**) closed conformation of the catalytic site between Trp47 and FMN412. For clarity, Trp47, FMN412 and the water molecule bound between them are shown in detail. The rest of protein is in the ribbon representation. Dashed lines are hydrogen bonds critical for the interaction between Trp47 and FMN412. Above corresponding figures, Trp47 and FMN412 are shown in the van der Waals representation. (**C**) Superposition of both conformations of the active site after alignment of the protein backbones. Structural changes occurring during the closing event are indicated by arrows.

sites Trp47-FMN412 and Trp253-FMN206 are symmetrical. We did not observe a difference in their behavior as well as no correlations between them, therefore in the remainder of text we will discuss only the situation around Trp47-FMN412. The same conclusions are valid for Trp253-FMN206.) We call this conformation "open" because substrate molecule can bind into the active site between Trp47 and FMN412 rings without significantly perturbing this conformation [Fig. 4(A)—the van der Waals representation]. The MD simulations allow the characterization of the static and dynamic features of biomolecules.[41] The water molecule stabilizing the open conformation of the active site is not rigidly bound to the catalytic site. A dynamic exchange of water molecules with an average residence time of 47 ps in the catalytic was observed in our MD study.

MD simulations also suggest other, more stable conformation of the catalytic site, which we call "closed" conformation. In this conformation, Trp47 and FMN412 are so close to each other that a substrate molecule is unable to bind between them without perturbing—"opening" this conformation [Fig. 4(B)—the van der Waals representation]. The distance between center of masses of the Trp47 and FMN412 rings decreased from about 0.9 nm (open conformation) to 0.5 nm (closed conformation) and surface accessible area of the pyrimidine part of FMN412 decreased from about $\approx$0.120 to $\approx$0.025 nm$^2$ (Fig. 5). For clarity, we present only the time scale of 0–5,000 ps in Figure 5, because there was no other opening of the active site after 2,000 ps in this selected MD run.

Opening and closing of the active site significantly modulate the accessibility of the isoalloxazine ring, i.e., Trp47 behaves like a gate toward the pyrimidine part of FMN412. Therefore, we called this gating mechanism as cofactor assisted. Opening and closing of the active site apparently has no significant effect on Rg, RMSD of the NOX backbone, and RMSD of the secondary structures; indicating no gross structural changes during open–close conformational transition (Figs. 1 and 3, and Fig. 1 in Supplementary Material).

The open and closed conformations could be differentiated by the distance between the planes of Trp47 and FMN412 [Fig. 5(A)]. The time dependence for one selected MD run of NOX in water reveals that the catalytic site closes during 500–570 ps, remains closed until 1,320 ps, reopens during 1,320–1,380 ps, remains open until 1,700 ps, closes during 1,700–1,750 ps, and remains closed until the end of the simulation (12,000 ps). The process of closing of the active site was very fast, $\approx$60 ps, and correlated with release of the bound water molecule from the active site. In the open conformation, the water molecule is strongly bound between Trp47 and FMN412 by two hydrogen bonds between the backbone NH group of Trp47 and the water oxygen and between the water and

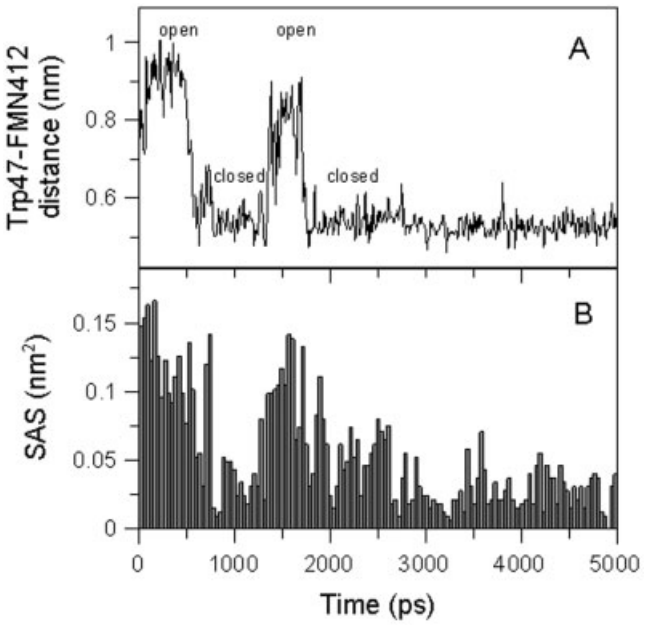


Fig. 5. Time evolution of (**A**) the distance between the center of masses of the indole ring of Trp47 and isoalloxazine ring of FMN412 in water solution; and (**B**) SAS of the pyrimidine part of the isoalloxazine ring.

oxygen of the hydroxyl group of FMN412 [Fig. 4(A)]. However, the water molecule is not present in the closed conformation of the active site, and the backbone NH group of Trp47 and the hydroxyl group of FMN412 are bound by a hydrogen bond [Fig. 4(B)]. A detailed analysis of the closing process shows that it occurred only when no water molecule was bound between Trp47 and FMN412 (i.e., when one water molecule went out and the next one was too slow to come into place before the closing event).

The structural difference between open and closed conformation [Fig. 4(C)] is mainly on the side of Trp47, which is shifted as whole residue toward FMN by about 0.2 nm, aiming in the formation of hydrogen bond between hydrogen of the backbone NH group of Trp47 and the oxygen of hydroxyl group of FMN412. Dihedral angle $\chi^1$ of Trp47 side-chain is not affected by closing of the active site and dihedral angle $\chi^{1,2}$ of Trp47 is changed by about 20°. Isoalloxazine ring of FMN412 is shifted only by 0.05 nm in the direction of the plane of ring. In the open conformation, the side-chain of Trp47 forms weak hydrophobic contacts with highly flexible helix F (namely, with residues Ala115, Ile116, Ala119, and Phe120). In the absence of water molecule bound between Trp47 and FMN412, these fluctuations are strong enough to induce approaching Trp47 closer to FMN412 and consequent closure of the active site.

In 10 independent simulations of NOX in water solution, we have observed closing of the active site in nine of them for the first catalytic site and in seven of them for the second catalytic site in the symmetrical unit. We do not see any correlation between closing the first and the second active site. In two runs, we observe not only closing event, but also reopening and after reclosing of the active site (Fig. 5). Two extra simulations using the electrostatic

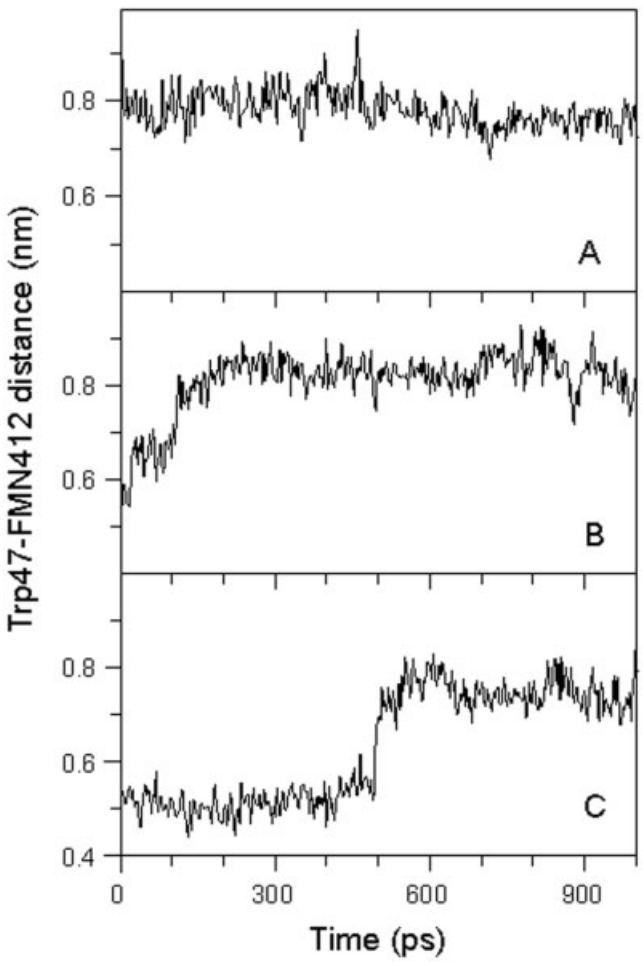


Fig. 6. Time evolution of the distance between the center of masses of the indole ring of Trp47 and the isoalloxazine ring of FMN412 in 1 M urea in three different MD runs. **A:** The initial structure was the crystal structure of NOX with the open catalytic site. In contrast, (B,C) the initial structure was the closed catalytic site of NOX in water solution. **B:** The initial position of urea 1 in Figure 7. **C:** Urea molecule diffused over a distance of ≈0.8 nm, approached to the proximity of the active site shown as the position of urea 2 in Figure 7.

treatments by PME were also performed. In these simulations, the same type of behavior as in the simulations using reaction-field treatment of electrostatic interactions was observed.

### Urea Molecule Stabilizes the Open State of the Active Site

In the presence of 1 M urea, the closing event was observed only in one from 10 MD simulations for this catalytic site in simulations of NOX [Fig. 6(A)]. Analysis of the MD trajectories of NOX in 1 M urea revealed the molecular mechanism that prevented closure of the catalytic site. In all MD simulations of NOX in water and 1 M urea, we have observed the fast binding of a urea molecule between Trp47 and FMN412, occurring in two steps. In the first step, the urea molecule formed a stable hydrogen bond coming from the carbonyl group to the water molecule bound between FMN and Trp47 in the active site. The

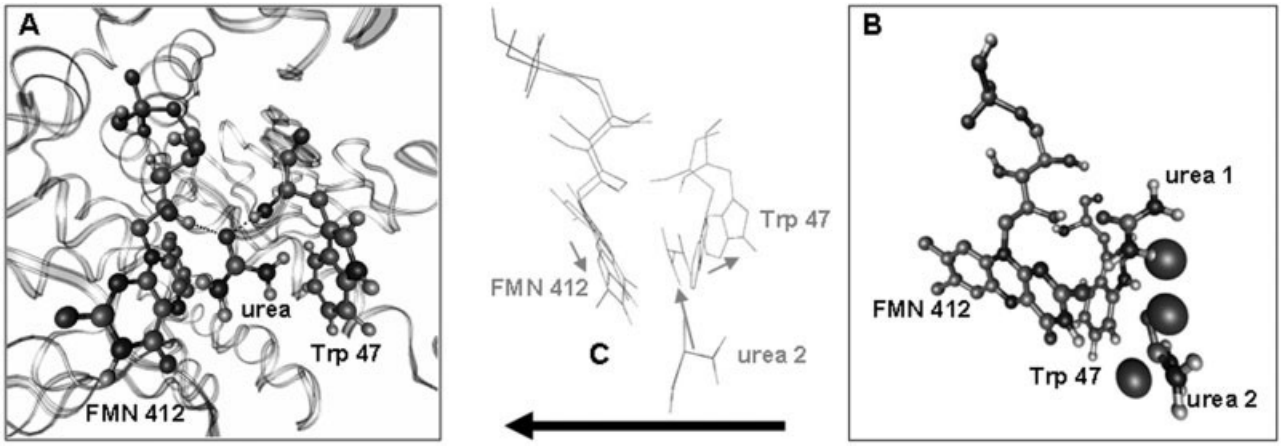


Fig. 7. Molecular model of the catalytic site of NOX in 1 M urea. **A:** The binding mode of urea in the active site of NOX. Trp47, FMN412, and urea are shown in detail. The rest of the protein is presented in the ribbon form. The hydrogen bonds stabilizing the position of the urea molecule between Trp47 and FMN412 are shown as dashed lines. **B:** Initial positions of the urea molecules (urea 1, urea 2, and dark balls) around the closed active site of NOX in 10 different MD runs. Positions of urea 1 and urea 2, with selected initial velocities of atoms, were productive, i.e., they induced the opening of the active site followed by their binding into it. In the rest of MD runs, the active site remained closed, urea molecules (dark balls) did not bind and moved away during the time of simulation. **C:** Superposition of both conformations of the active site after alignment of the protein backbones. Structural changes occurring during the opening event induced by the binding of the urea 2 molecule are indicated by arrows.

average residence time of such a complex was 40 ps. After the formation of this complex, the orientation of the water molecule changed and was not favorable to form both the hydrogen bonds to Trp47 and FMN412, as in the absence of urea. The position of the bound urea molecule was stabilized by two hydrogen bonds coming from the backbone NH group of Trp47 (98%) and the hydroxyl group of FMN412 (92%) to the carbonyl group of urea [Fig. 7(A)]. The percentage values represent the percentage of the time the hydrogen bond occurred over the total time of the simulation.[41] This binding is relatively strong because, after the binding of urea between Trp47 and FMN412, we have not seen its release from the catalytic site over the duration of the 12/18 ns MD simulations. The bound urea prohibits the closure of the catalytic site because of steric restraints [Fig. 7(A)].

From the overall 10 independent MD simulations of NOX in urea solution, the binding of urea molecule was observed in nine independent runs for the first catalytic site and in 10 independent runs for the second catalytic site. In the case in which urea was not bound, the catalytic site closed before urea entered this region.

### Urea Unlocks the Already Closed Active Site

We were interested in whether a urea molecule is able to bind into the active site even when the active site is closed. We have tested this in the following way: the structure of NOX with a closed active site (Trp47—FMN412) has been taken from the simulation in water and incorporated into the 1 M urea solution. The simulations revealed that there is a much narrower space in the closed than in the open conformation (see Fig. 4) for the urea molecules. A simple MD simulation is not able to sample all possible conformations of the urea molecule around the catalytic site of NOX (our time limit is about 18 ns). With the aim of sampling the relevant region around the active site, we performed 10 independent MD run in which five different initial positions for the urea molecule in close proximity to the Trp47—FMN412 site have been chosen [urea 1, urea 2, and dark balls on Fig. 7(B)]. For each initial configuration, we have run two independent MD runs using different initial velocities of atoms. Positions of the urea 1 and urea 2, with selected initial velocities of atoms, were productive, i.e., these molecules of urea induced opening of the active site and bound into it.

Starting from the initial position of urea 1 [Fig. 7(B)], we have observed its slow incorporation between the indole ring of Trp47 and isoalloxazine ring of FMN412. Figure 6(B) shows the slow opening of the active site of NOX between the planes of Trp47 and FMN412 in 1 M urea. In the next step, the same binding mode of urea was formed as in simulations, starting with the open conformation of the catalytic site of NOX (formation of two hydrogen bonds between the carbonyl group of urea and the backbone NH group of Trp47 and the hydroxyl group of FMN412) (Fig. 7A).

In another MD run from this set of simulations, urea put into close proximity to the binding site did not bind. However, the urea molecule distanced 0.8 nm from the active site diffused in the proximity of the catalytic site during the simulation time [position urea 2, Fig. 7(B)]. In the following step it incorporated between rings of Trp47 and FMN412 within 10 ps [Fig. 6(C)], where it formed stable hydrogen bonds with the backbone NH group of Trp47 and the hydroxyl group of FMN412, i.e., the same binding mode of urea within the catalytic binding site as was observed in the bindings into the "open" catalytic site [Fig. 7(A)].

In all others MD runs within this simulation set, we did not observe urea-induced opening of the active site. However, in two of the MD runs, spontaneous opening was

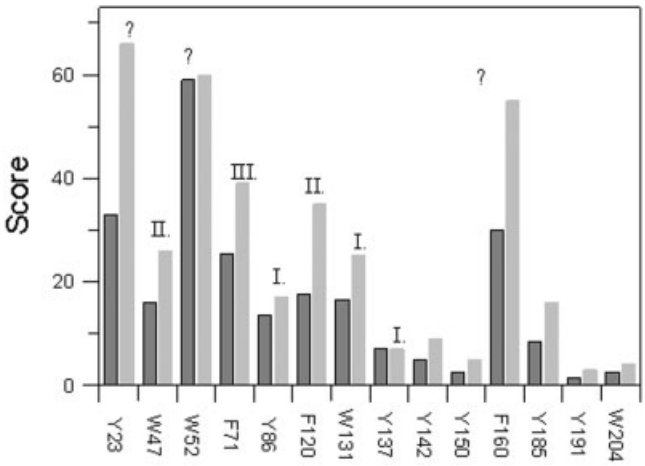


Fig. 8. Clusters of the aromatic residues around flavin cofactor from superposition of the different nitroreductases, flavin reductases, and NOX. There are three main clusters lining the *re*-side of flavin cofactor: (I) xylene part, (II) above middle part of isoalloxazine ring, and (III) close to the rim of pyrimidine ring. The question marks indicate conserved positions of aromatic residues without evident relation to the active site. Light bars correspond to simple counts (see Material and Methods), dark bars correspond to counts weighted by factor that takes into account different number of the codons for aromatic amino acids.

followed by urea binding between Trp47 and FMN412 cofactor.

### Conservation of Aromatic Positions in the Primary Sequence of NOX From *T. thermophilus*

There are 14 aromatic residues per monomer: four tryptophans (W47, W52, W131, W204), seven tyrosines (Y23, Y86, Y137, Y142, Y150, Y185, Y191) and three phenylalanines (F71, F120, F160). Based on the multiple sequence alignment, degree of conservation was calculated (Fig. 8). The three most conservative aromatic positions are of the Trp52, Phe160, and Phe71. Conservation of the aromatic residue at the position of Trp47 is only modest. Similarly, aromatic residues lining the active site on the *re*-side of the flavin are only modestly conserved. Primary sequence analysis reveals weak conservation of the residues that may be part of the gating mechanism. However, based on the analysis of three-dimensional protein structures, there are various possibilities for how to place bulky aromatic residue and modulate flavin accessibility, e.g., position of the Trp47 in NOX from *T. thermophilus* is similar with the position of Phe124 in nitroreductase from *E. coli*.

## DISCUSSION

NOX from *T. thermophilus*, as a potentially interesting enzyme for biotechnological applications, has been successfully cloned and purified.[20,21,42] Isolation of the overproduced protein in reasonable amounts allowed for crystallization and systematic characterization of this thermostable flavoenzyme.[4,43] Recently, the effect of solvent composition (e.g., urea, salts, pH) on the activity of NOX has been intensively investigated.[17–19] The enzyme was characterized by means of standard protein biophysical-biochemical techniques: (a) CD in the far-UV and the near-UV regions; (b) tryptophan and flavin fluorescence; (c) fluorescence quenching; and (d) activity measurements.

We have shown that perturbation of the enzyme active site by 1 M urea or a change in the pH of the protein solution from pH 7.0 to 5.0 led to a ~2.5- and ~2.0-fold increase in the enzyme activity, respectively.[17,19] Results obtained from CD showed that the global conformation of the protein was unaffected by 1 M urea[17] which is in agreement with current results from MD [Fig. 1, Fig. 1(A,B) in Supplementary Material]. A similar observation, the stimulatory effect of low concentrations of chaotropic agents on the activity of certain enzymes, has been reported in several articles.[44–48] Modulation of the activity of NOX can be even more sensitively tuned by anions of the Hofmeister series. The data demonstrate that the high rigidity of the active site in the presence of kosmotropic anions, and its great flexibility in the presence of chaotropic anions each have a decelerating effect on the enzyme activity.[18]

B-factors, as markers of the flexibility, obtained from X-ray diffraction were compared with those obtained from MD of NOX in water. Good correlation was found and the pattern of distribution of B-factors was similar (corresponding Pearson's correlation coefficient is 0.8491). The reasons for some deviations follow from: (1) comparison of protein structures at different conditions, i.e., MD simulations performed in water have been compared with protein structure from the crystal form; (2) crystal defects[33]; and (3) difficulty in sampling enormous number of degrees of freedom of all protein conformations by MD. Comparison of the B-factors calculated for MD trajectories of NOX in the absence and presence of urea shows that 1 M urea does not significantly affect global backbone flexibility (corresponding Pearson's correlation coefficient is 0.8360) which is in accordance with previous experimental results.[17] To analyze some differences in dynamical behavior of NOX in water and 1 M urea solution we have also calculated time evolution of RMSDs of the 17 secondary structure elements over time. The RMSDs of secondary structure elements indicate that the secondary structure of NOX is not significantly affected by the addition of 1 M urea (Fig. 3).

Our MD study is the first one that suggests the existence of both open and closed conformations of the active sites in NOX as well dynamic exchange between them—gating mechanism. Noteworthy, authors of the X-ray structure of NOX emphasized inherent dynamics of the enzyme active site: "elevated temperature factors and weaker electron density of side chain of Trp47 indicates flexibility."[4] Another experimental finding suggesting the possibility of a similar gating mechanism was observed in structurally closed flavoprotein—nitroreductase from *E. coli* that was crystallized in free and substrate bound form (nicotinic acid). It revealed local movement of Phe124, analogous to Trp47 in NOX, upon binding of the nicotinic ring.[14] The binding site of nicotinic acid is blocked by bulky phenylalanine and after binding of substrate Phe124 shifts away from the binding site because of sterical repulsion.

The MD simulations provide a possible interpretation of previous experimental results of the specific effect of 1 M urea on NOX from *T. thermophilus*. Based on our experimental findings and structural considerations, we suggested a role for Trp47 as a switch that regulates substrate entering and the product leaving the catalytic site. This requires that Trp47 be kept in the proper position toward the isoalloxazine ring by the tightly bound water molecule. This suggestion is supported by the analogous role of the tryptophan residue in the nonhomologous NADPH-cytochrome P450 oxidoreductase.[15] The MD simulations presented further support for the existence of a sandwich-like conformation of Trp47, water, and the isoalloxazine ring in NOX. In fact, the ability of urea to replace water in the active site and to stabilize the open conformation may be linked with the changes in activity of NOX in 1 M urea. We have observed two different pathways of urea binding into active site: (1) urea binds directly into open conformation of the active site; and (2) urea induces opening of the active site and binds into it.

However, the role of the bound urea molecule seems to be dual. Urea keeping the active site open increases the turnover rate and, simultaneously, urea occupying the active site can slow down substrate binding. Apparently, the urea molecule is not bound so tightly that this effect would overcome the effect of stabilization of the open conformation. The MD simulations indicate a primary role for the carbonyl oxygen in urea entering and being stabilized in the active site. The revealed details of the molecular mechanism of urea binding the active site of NOX can contribute to the design of efficient modulators of NOX activity. Interestingly, urea structurally mimics part of the nicotinamide group of the substrate molecule and suggests a mode of substrate binding.

## Application to the Homologous Nitroreductase/Flavin Reductase Family

The presented cofactor assisted gating mechanism may be valid for the entire family of nitroreductases and flavin reductases. Six published crystallographic structures from this interesting flavoprotein family are known.[1] The overall folding, tertiary structure, and the occurrence of secondary structures in nitroreductases, and the unusually large interlocking dimeric interfaces of flavin reductases and NOX, are similar: they are composed of at least two domains containing segregated $\alpha + \beta$ regions. Significant structural differences are observed only in a few residues, mostly from helix G and the surface loops. These residues are very flexible and possibly convey substrate specificity.[2,8] It seems likely that the differences in substrate specificities are attributable to the divergent evolution of a common ancestral flavoprotein. Nevertheless, the $\alpha$-$\beta$-$\alpha$-$\beta$ core regions and the active sites of the nitroreductases, the flavin reductases, and NOX from *T. thermophilus* contain a high degree of structural similarity.[49]

We focused on the active site and the occurrence of aromatic residues within this family. The flavin rings (active sites) of the homologous flavoproteins (NOX from *T. thermophilus*—1nox, NADPH:FMN oxidoreductase from *Vibrio harveyi*—1bkj, NAD(P)H:FMN oxidoreductase from *Vibrio fisheri*—1vfr, nitroreductase from *Enterobacter cloacae*—1nec, FMN-dependent nitroreductase from *E. coli* B—1ds7, oxygen-insensitive NADPH nitroreductase from *E. coli*—1f5v) were superimposed (Fig. 9). There are three clusters of aromatic residues covering different parts of the isoalloxazine ring on the *re*-side: (I) the xylene part of the ring is covered mostly by tryptophanes: Trp131 (1nox), Trp137 (1nec), Phe86 (1f5v), and Trp138 (1ds7); (II) the middle part, i.e., the position of Trp47 in NOX (1nox), is covered mostly by the phenylalanines: Phe123, Phe124 (1ds7), Phe123 (1nec), Phe124 (1vfr), and; (III) the rim of the pyrimidine part is covered by phenylalanines only: Phe71 (1nox), Phe72 (1vfr), Phe70 (1df7), Phe69 (1nec), Phe63 (1bkj). We noted that some of the flavoproteins possess aromatic residues on the *si*-side of the flavin such as NADPH:FMN oxidoreductase from *V. harveyi*. The common presence of aromatic residues near the active site seems to be significant at ~40% pair-wise sequence identities. In addition, the matrix of relative substitution frequencies shows that the aromatic residues form one exchange group with similar properties.[50] A cluster of aromatic residues covering the middle position of the isoalloxazine ring contained Trp47. The present study shows that Trp47 serves as a molecular gate. The function of the aromatic residues may be similar, i.e., modulation of the solvent/substrate accessibility of active sites of flavoproteins by a gating mechanism.

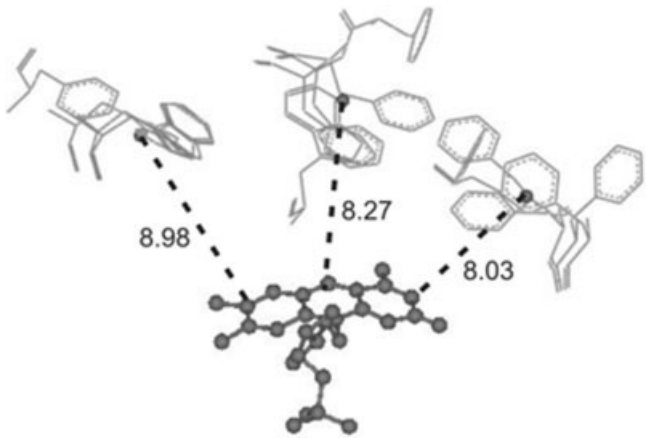


Fig. 9. Degree of the conservation for the position of the aromatic residues in the primary structure of NOX. Based on the structure analysis (Fig. 8), there are three main clusters lining the *re*-side of flavin cofactor: (I) xylene part, (II) above middle part of isoalloxazine ring, and (III) close to the rim of the pyrimidine ring.

It should be noted that aromatic residues actively take part also in the gating mechanism in various unrelated enzymes, e.g., acetylcholinesterase, potassium channels, and cytochrome-P450.[51–53] The detailed MD simulations of acetylcholinesterase show that the concerted motion of a large number of residues contributes to opening the bottleneck and makes a free path for the substrate molecule.[51,54] Analysis of the time resolved fluorescence anisotropy revealed the importance of random segmental movements in the transient opening.[55]

The participation of aromatic amino acids in the gating mechanisms of flavoproteins is probably a result of their properties: (i) the rotation barriers of aromatic residues are relatively low[56,57]; (ii) aromatic residues are the largest amino acid residues and efficiently fill the open entrance to the active site; and (iii) the weakly polar properties of the aromatic amino acids[58] also facilitate their localization in the interface region of proteins.

The described molecular mechanism for the activity enhancement of NOX by the addition of urea at room temperature serves not only to further understanding of enzymatic activity, but can also be used in biotechnological applications of the nitroreductases.

## CONCLUSION

MD simulations of NOX in water and in 1 M urea indicate close resemblance of structure and protein backbone dynamics of the enzyme. They revealed the cofactor assisted gating process of the catalytic site between Trp47 and FMN412 on a detailed atomic level. The binding of the urea molecule between the planes of Trp47 and FMN412 prohibits closure of the catalytic site and provides a possible explanation of the observed increase in NOX activity induced at low urea concentrations. The presented molecular modeling data are in good agreement with our previous experimental results and confirm the proposal that: (i) Trp47 is important for enzyme catalysis and substrate binding, and (ii) urea opens the active site without perturbing the overall structure of the protein.[17]

## ACKNOWLEDGMENTS

The authors are thankful for the support of the European Community-Research Infrastructure Action under the FP6 "Structuring the European Research Area" Program for sponsoring research stay of J.H. in the SARA supercomputer center in Amsterdam. They also thank Linda Sowdal for her invaluable editorial help in preparing the manuscript and Dr. Chris Oostenbrink for valuable discussions.

## REFERENCES

1. Murzin AG, Brenner SE, Hubbard T, Chothia C. SCOP: a structural classification of proteins database for the investigation of sequences and structures. J Mol Biol 1995;247:536–540.
2. Tanner JJ, Lei B, Tu SC, Krause KL. Flavin reductase P: structure of a dimeric enzyme that reduces flavin. Biochemistry 1996;35: 13531–13539.
3. Haynes CA, Koder RL, Miller AF, Rodgers DW. Structures of nitroreductase in three states: effects of inhibitor binding and reduction. J Biol Chem 2002;277:11513–11520.
4. Hecht HJ, Erdmann H, Park HJ, Sprinzl M, Schmid RD. Crystal structure of NADH oxidase from *Thermus thermophilus*. Nat Struct Biol 1995;2:1109–1114.
5. Bryant C, DeLuca M. Purification and characterization of an oxygen-insensitive NAD(P)H nitroreductase from *Enterobacter cloacae*. J Biol Chem 1991;266:4119–4125.
6. Zenno S, Koike H, Kumar AN, Jayaraman R, Tanokura M, Saigo K. Biochemical characterization of NfsA, the *Escherichia coli* major nitroreductase exhibiting a high amino acid sequence homology to Frp, a *Vibrio harveyi* flavin oxidoreductase. J Bacteriol 1996;178:4508–4514.
7. Lei B, Tu SC. Mechanism of reduced flavin transfer from *Vibrio harveyi* NADPH-FMN oxidoreductase to luciferase. Biochemistry 1998;37:14623–14629.
8. Parkinson GN, Skelly JV, Neidle S. Crystal structure of FMN-dependent nitroreductase from *Escherichia coli* B: a prodrug-activating enzyme. J Med Chem 2000;43:3624–3631.
9. Dachs GU, Tupper J, Tozer GM. From bench to bedside for gene-directed enzyme prodrug therapy of cancer. Anticancer Drugs 2005;16:349–359.
10. Palmer DH, Chen MJ, Searle PF, Kerr DJ, Young LS. Inhibition of NF-kappaB enhances the cytotoxicity of virus-directed enzyme prodrug therapy and oncolytic adenovirus cancer gene therapy. Gene Ther 2005;12:1187–1197.
11. Best EP, Kvesitadze GK, Khatisahvili G, Sadunishvili T. Plant processes important for the transformation and degradation of explosives contaminants. Z Naturforsch 2005;60:340–348.
12. Kurumata M, Takahashi M, Sakamotoa A, et al. Tolerance to, and uptake and degradation of 2,4,6-trinitrotoluene (TNT) are enhanced by the expression of a bacterial nitroreductase gene in *Arabidopsis thaliana*. Z Naturforsch 2005;60:272–278.
13. Koike H, Sasaki H, Kobori T, et al. 1.8 A crystal structure of the major NAD(P)H:FMN oxidoreductase of a bioluminescent bacterium, *Vibrio fischeri*: overall structure, cofactor and substrate-analog binding, and comparison with related flavoproteins. J Mol Biol 1998;280:259–273.
14. Lovering AL, Hyde EI, Searle PF, White SA. The structure of *Escherichia coli* nitroreductase complexed with nicotinic acid: three crystal forms at 1.7 A, 1.8 A, and 2.4 A resolution. J Mol Biol 2001;309:203–213.
15. Hubbard PA, Shen AL, Paschke R, Kasper CB, Kim JJ. NADPH-cytochrome P450 oxidoreductase. Structural basis for hydride and electron transfer. J Biol Chem 2001;276:29163–29170.
16. Zhang J, Martásek P, Paschke R, Shea T, Siler Masters BS, Kim JJ. Crystal structure of the FAD/NADPH-binding domain of rat neuronal nitric-oxide synthase. Comparisons with NADPH-cytochrome P450 oxidoreductase. J Biol Chem 2001;276:37506–37513.
17. Žoldák G, Šuťák R, Antalík M, Sprinzl M, Sedlák E. Role of conformational flexibility for enzymatic activity in NADH oxidase from *Thermus thermophilus*. Eur J Biochem 2003;270:4887–4897.
18. Žoldák G, Sprinzl M, Sedlák E. Modulation of activity of NADH oxidase from *Thermus thermophilus* through change in flexibility in the enzyme active site induced by Hofmeister series anions. Eur J Biochem 2004;271:48–57.
19. Žoldák G, Musatov A, Stupák M, Sprinzl M, Sedlák E. pH-induced changes in activity and conformation of NADH oxidase from *Thermus thermophilus*. Gen Physiol Biophys 2005;24:279–298.
20. Park HJ, Kreutzer R, Reiser CO, Sprinzl M. Molecular cloning and nucleotide sequence of the gene encoding a H2O2-forming NADH oxidase from the extreme thermophilic *Thermus thermophilus* HB8 and its expression in *Escherichia coli*. Eur J Biochem 1992;205:875–879.
21. Park HJ, Reiser CO, Kondruweit S, Erdmann H, Schmid RD, Sprinzl M. Purification and characterization of a NADH oxidase from the thermophile *Thermus thermophilus* HB8. Eur J Biochem 1992;205:881–885.
22. Berman HM, Westbrook J, Feng Z, et al. The Protein Data Bank. Nucleic Acids Res 2000;28:235–242.
23. van Gunsteren WF, Billeter SR, Eising AA, et al. Biomolecular simulation: the Gromos96 manual and user guide. Zurich, Switzerland: Hochschulverlag AG an der ETH Zurich; 1996.
24. Berendsen HJ, van der Spoel D, van Drunen R. GROMACS: a message-passing parallel molecular dynamics implementation. Comput Phys Commun 1995;95:43–56.
25. Lindahl E, Hess B, Van der Spoel D. Gromacs 3.0: a package for molecular simulation and trajectory analysis. J Mol Mod 2001;7: 306–317.
26. Berendsen HJC, Postma JPM, van Gunsteren WF, Hermans J. Interaction models for water in relation to protein hydratation. In: Pullman B, editor. Intermolecular forces. Dordrecht: D. Reidel Publishing;1981. p 331–342.
27. Verlet L. Computer "experiments" on classical fluids. I. Thermodynamical properties of Lennard-Jones molecules. Phys Rev 1967; 159:98–103.
28. Hess B, Bekker H, Berendsen HJ, Fraaije JGEM. LINCS: a linear constraint solver for molecular simulations. J Comput Chem 1997;18:1463–1472.
29. Miyamoto S, Kollman PA. Settle: an analytical version of the SHAKE and RATTLE algorithm for rigid water models. J Comput Chem 1992;13:952–962.

30. Berendsen HJC, Postma JPM, DiNola A, Haak JR. Molecular dynamics with coupling to an external bath. J Chem Phys 1984;81:3684–3690.
31. Tironi I, Sperb R, Smith PE, van Gunsteren WF. A generalized reaction field method for molecular dynamics simulations. J Chem Phys 1995;102:5451–5459.
32. Essmann U, Perera L, Berkowitz LA. Smooth particle mesh Ewald method. J Chem Phys 1995;103:8577–8593.
33. Carugo O, Argos P. Accessibility to internal cavities and ligand binding sites monitored by protein crystallographic thermal factors. Proteins 1998;31:201–213.
34. Lee B, Richards FM. The interpretation of protein structures: estimation of static accessibility. J Mol Biol 1971;55:379–400.
35. Kabsch W, Sander C. Dictionary of protein secondary structure: pattern recognition of hydrogen-bonded and geometrical features. Biopolymers 1983;22:2577–2637.
36. Humphrey W, Dalke A, Schulten K. VMD: visual molecular dynamics. J Mol Graphics 1996;14:33–38.
37. Thompson JD, Higgins DG, Gibson TJ. CLUSTAL W: improving the sensitivity of progressive multiple sequence alignment through sequence weighting, position-specific gap penalties and weight matrix choice. Nucleic Acids Res 1994;22:4673–4680.
38. Berman HM, Westbrook J, Feng Z, et al. The Protein Data Bank. Nucleic Acids Res 2000;28:235–242.
39. Karplus M, Petsko GA. Molecular dynamics simulations in biology. Nature 1990;347:631–639.
40. García AE. Large-amplitude nonlinear motions in proteins. Phys Rev Lett 1992;68:2696–2699.
41. Hritz J, Uličný J, Laaksonen A, Jancura D, Miškovský P. Molecular interaction model for the C1B domain of protein kinase C-gamma in the complex with its activator phorbol-12-myristate-13-acetate in water solution and lipid bilayer. J Med Chem 2004;47:6547–6555.
42. Park HJ, Kreutzer R, Reiser CO, Sprinzl M. Molecular cloning and nucleotide sequence of the gene encoding a H2O2-forming NADH oxidase from the extreme thermophilic *Thermus thermophilus* HB8 and its expression in *Escherichia coli*. Eur J Biochem 1993;211:909.
43. Erdmann H, Hecht HJ, Park HJ, Sprinzl M, Schomburg D, Schmid RD. Crystallization and preliminary X-ray diffraction studies of a NADH oxidase from *Thermus thermophilus* HB8. J Mol Biol 1993;230:1086–1088.
44. Fan YX, Ju M, Zhou JM, Tsou CL. Activation of chicken liver dihydrofolate reductase by urea and guanidine hydrochloride is accompanied by conformational change at the active site. Biochem J 1996;315:97–102.
45. Zhang HJ, Sheng XR, Pan XM, Zhou JM. Activation of adenylate kinase by denaturants is due to the increasing conformational flexibility at its active sites. Biochem Biophys Res Commun 1997;238:382–386.
46. Narayanasami R, Nishimura JS, McMillan K, et al. The influence of chaotropic reagents on neuronal nitric oxide synthase and its flavoprotein module. Urea and guanidine hydrochloride stimulate NADPH-cytochrome c reductase activity of both proteins. Nitric Oxide 1997;1:39–49.
47. Das M, Dasgupta D. Enhancement of transcriptional activity of T7 RNA polymerase by guanidine hydrochloride. FEBS Lett 1998;427:337–340.
48. Inui T, Ohkubo T, Urade Y, Hayaishi O. Enhancement of lipocalin-type prostaglandin D synthase enzyme activity by guanidine hydrochloride. Biochem Biophys Res Commun 1999;266:641–646.
49. Watanabe M, Nishino T, Takio K, Sofuni T, Nohmi T. Purification and characterization of wild-type and mutant "classical" nitroreductases of *Salmonella typhimurium*. L33R mutation greatly diminishes binding of FMN to the nitroreductase of *S. typhimurium*. J Biol Chem 1998;273:23922–23928.
50. Schulz GE, Schirmer RH. Principles of protein structures. New York: Springer Verlag; 1984.
51. Shen T, Tai K, Henchman RH, McCammon JA. Molecular dynamics of acetylcholinesterase. Acc Chem Res 2002;35:332–340.
52. Kanevsky M, Aldrich RW. Determinants of voltage-dependent gating and open-state stability in the S5 segment of Shaker potassium channels. J Gen Physiol 1999;114:215–242.
53. Winn PJ, Ludemann SK, Gauges R, Lounnas V, Wade RC. Comparison of the dynamics of substrate access channels in three cytochrome P450s reveals different opening mechanisms and a novel functional role for a buried arginine. Proc Natl Acad Sci USA 2002;99:5361–5366.
54. Zhou HX, Wlodek ST, McCammon JA. Conformation gating as a mechanism for enzyme specificity. Proc Natl Acad Sci USA 1998;95:9280–9283.
55. Boyd AE, Dunlop CS, Wong L, Radic Z, Taylor P, Johnson DA. Nanosecond dynamics of acetylcholinesterase near the active center gorge. J Biol Chem 2004;279:26612–26618.
56. Gelin BR, Karplus M. Sidechain torsional potentials and motion of amino acids in proteins: bovine pancreatic trypsin inhibitor. Proc Natl Acad Sci USA 1975;72:2002–2006.
57. McCammon JA, Karplus M. Dynamics of activated processes in globular proteins. Proc Natl Acad Sci USA 1979;76:3585–3589.
58. Burley SK, Petsko GA. Weakly polar interactions in proteins. Adv Protein Chem 1988;39:125–189.